

# The Influence of Thermal Irradiation Synchronously Aging on the Structure of Modified Sodium Bentonite

Wei Liu, Shuaiwei Zhao, Liang Dong, Zhontian Yang, Honghui Li, Jianqin Liu and Lei Wan

**Abstract** In order to study the influence of thermal irradiation ( $\gamma$ ) synchronously aging on the properties of bentonite, the Gaomiaozhi(GMZ)-modified sodium bentonite was investigated by heating (90 °C) and irradiating(dose rates 85, 170, 610 Gy/h; cumulative doses 0.28, 0.37, 0.74 MGy). The results of thermal analysis and XRD showed that the influence of heating and irradiating on the thermal properties, phase components, and structures of the GMZ-modified sodium bentonite is no obvious, the  $\gamma$ -ray cumulative dose effects and dose rate effects are generally weak.

**Keywords** Modified sodium bentonite · Thermal irradiation synchronously aging · Gamma cumulative dose effect · Dose rate effect

## 1 Introduction

Clay minerals are of crucial importance in the safety and long-term performance of underground high-level radioactive waste disposal concepts. The major component of engineered barriers is bentonite. The bentonite is affected by the heat and irradiation that produced from the waste, so it is crucial to investigate the influence of heat and irradiation on the properties of bentonite.

The changes of physico-chemical properties are caused by the effect of heat and irradiation. The stability of Al-O and Si-O band is destroyed by irradiation, so defects are formed in the crystal structure [1, 2]. Gournis et al. [3] found that the radiation induces paramagnetic defect centers. The results of [4, 5] indicated the concentration of the defect depends on the granulometrical fraction (clay fraction or coarse fraction), the coarse fraction has a higher concentration in defects than the clay fraction, and the concentration of radiation-induced defects increased with

---

W. Liu (✉) · S. Zhao · L. Dong · Z. Yang · H. Li · J. Liu · L. Wan  
CNNC Key Laboratory on Geological Disposal of High-Level Radioactive Waste,  
China Institute for Radiation Protection, Taiyuan 030006, China  
e-mail: fflglw@126.com

increasing dose. The concentration of the defects is even more sensitive in the presence of mobile water molecules [6]. Moreover, after the effects of heat and irradiation, the crystal particle size decreases [7, 8]; this creates an increased specific surface area [8], and in addition, the property swelling is alterative [9, 10] found the GMZ-modified sodium bentonite maintains its ability of water absorption after  $\gamma$  irradiation for 5 MGy, then thermal aging for 1 year at 230 °C. Due to radiolysis of the interlayer and pore water, it generates the redox species that can result the change of valence state for iron (form  $\text{Fe}^{3+}$  to  $\text{Fe}^{2+}$ ); this may alter the swelling property, CEC, specific surface area, and layer charge [9, 11, 12]. The transformation of the dissolution and adsorption about nuclides is caused by irradiation,  $\text{Al}^{3+}$  ions decreases,  $\text{Si}^{4+}$  ions increases [6], and the adsorption capacity for  $^{137}\text{Cs}^+$  decreases [9, 13] found that the GMZ-modified Na bentonite was more stable than natural Ca bentonite during both thermal aging and electron irradiation aging, and it was appropriate to chose natural Na bentonite or modified Na bentonite as buffer material.

In the former study, the great dose rates (form several hundred Gy/h to several tens kGy/h) and large cumulative doses (form several MGy to 30 MGy) were used to study the cumulative dose effects on clay minerals, but there are few studies on the effect of dose rate. This is because that the initial surface dose rates of the waste containers are about 2 Gy/h and drop off by an order of magnitude within 200 years [11, 14]; it is unrealistic that the samples received large cumulative doses are obtained by using such small dose rates in laboratory experiment. So, in the present work, in order to be close to the true conditions, the GMZ-modified sodium bentonite was irradiated by small dose rates (from several tens Gy/h to several hundred Gy/h), and the influence of heat and irradiation (includes the effects of cumulative doses and dose rates) on the structure is investigated.

## 2 Methods and Materials

In the present work, the GMZ-modified sodium bentonite [7] was investigated, and the average water content is 8.62%.

The samples were packed in closed buckets that were made of iron and wrapped by self-temperature limiting heating belt, and the thickness of the container is 1 mm. They were irradiated at 90 °C in  $^{60}\text{Co}$  gamma sources of 37,000 Ci, and the irradiated conditions were listed in Table 1.

After aging, the samples were analyzed by thermal analysis (NETZSCH STA449F3, parameters: platinum crucible with cover, nitrogen-30 ml/min, heating rate 10 °C/min, mass  $16 \pm 0.5$  mg) and X-ray diffraction(XRD) (Dandong haoyuan DX2700;  $\text{CuK}\alpha$ , range 4–70°2 $\theta$ , step size 0.02°, counting time 1 s or 3 s).

**Table 1** Experimental conditions

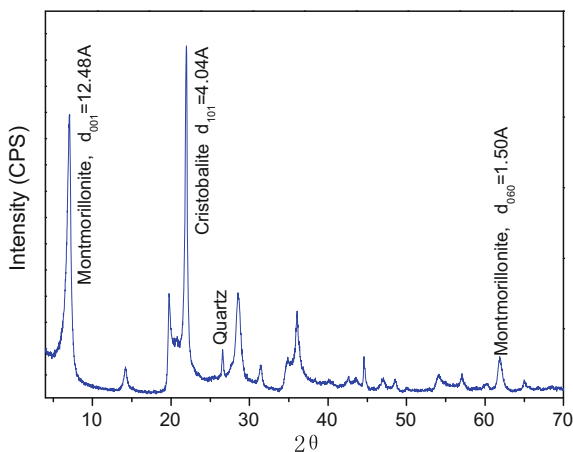
Sample ID	Experimental conditions		Exposed time (h)
	$\gamma$ -exposed rate (Gy/h)	$\gamma$ -irradiated dose (MGy)	
1#	85	0.28	3294
2#	85	0.37	4353
3#	170	0.37	2176
4#	170	0.74	4353
5#	610	0.37	607
6#	Reference		

### 3 Results and Discussion

#### 3.1 The Analyses of Reference (6#) Sample

The GMZ-modified sodium bentonite mostly contains montmorillonite and cristobalite, and trace quartz (Fig. 1). The  $d_{001}$  of montmorillonite is 12.48 Å, constancy with one layer of water molecule in the interlayer, and the  $d_{060}$  is 1.50 Å, so this sample is indeed dioctahedral mineral. This sample has the similar curve of differential scanning calorimetry(DSC) for Smectite minerals [15]; in the range of 25–950 °C, there are three endothermic valleys (Fig. 2); and in the range of 50–150 °C, the shape and bulk of the valley reflect function for water absorption/dehydration to some extent [15]. In the DSC curve, the first endothermic valley is big, so the sample contains some water; this corresponds with water content 8.62% in the sample. In the range of 530–750 °C, it has the second endothermic valley and also corresponds with another mass loss step in TG curve, and it primarily loses crystal water in this stage. The peak temperature of the second endothermic valley reflects the thermal stability of bentonite [15]. In the range of

**Fig. 1** XRD spectra of reference sample



830–910 °C, it has the third endothermic valley, and there is no obvious mass loss step; the structure of bentonite breaks up in the stage.

### 3.2 The Thermal Analyses of Aged Samples

The samples have the similar TG curves, so there is a representative line in following thermal curve pictures.

#### 3.2.1 The Analyses of Aged Samples with Different Accumulative Doses

The DSC curves between 6# sample and aged samples (1#, 2#, 3#, 4#) are basic agreement (Figs. 3 and 4), there are three endothermic valleys, and they have similar TG curves with two mass loss steps (Figs. 3 and 4). But, they have some discrepancies of the peak shape and peak area for the first endothermic valleys, which indicate that the surface and interlayer water content of the samples before and after aging has some difference, and this is due to gamma ray induced part of water radiolysis [16] and water evaporation caused by long-term effect at high temperature (90 °C).

According to the data (Table 2), it is obvious that the peak temperatures of the first endothermic valley for aged samples are lower than 6# sample; this is because the surface and interlayer water content decreases after aging, and the peak temperatures of the second and third endothermic valley are almost constant, all close to 690 °C for the second peak temperature and 880 °C for the third peak temperature; they indicate that the thermal stability and skeleton construction of all samples are basically unchanged. But, the endothermic values of the second endothermic valley for aged samples are lower (reduced 11–19% compared to 6#

**Fig. 2** Thermal curve of reference sample

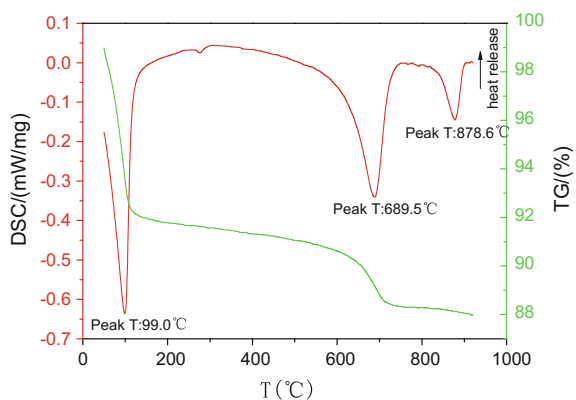


**Fig. 3** Thermal curve of Na bentonite with different cumulative dose at 85 Gy/h

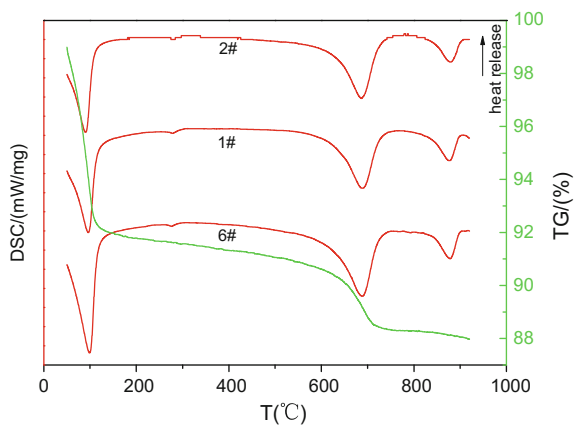


**Fig. 4** Thermal curve of Na bentonite with different cumulative dose at 170 Gy/h

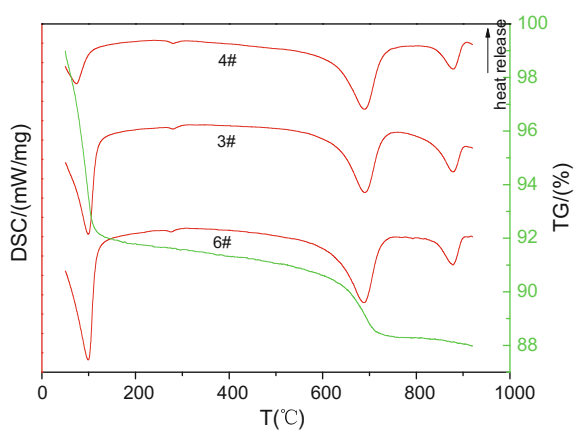
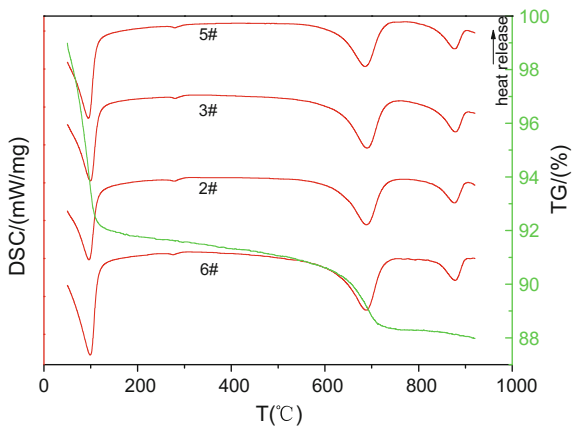


**Table 2** Thermal results of Na bentonite after aging

Samples ID	The 1st endothermic valley	The 2nd endothermic valley		The 3rd endothermic valley	
	Peak T (°C)	Peak T (°C)	Endothermic value (J/g)	Peak T (°C)	Endothermic value (J/g)
6#	99.0	689.5	168.20	878.6	36.02
1#	95.4	687.7	136.40	878.2	36.62
2#	88.7	687.0	149.70	879.8	33.87
3#	96.9	690.1	149.30	878.8	40.23
4#	71.9	687.9	144.60	879.3	33.38
5#	93.4	686.7	125.70	877.6	35.24

**Fig. 5** Thermal curve of Na bentonite with different dose rate at 0.37 MGy



sample) than 6# sample, so it seemingly indicates that effect of aging influences the crystal water of modified sodium bentonite.

### 3.2.2 The Analyses of Aged Samples with the Same Accumulative Doses but Different Dose Rates

There are also similar thermal curve between the aged samples and 6# sample (Fig. 5), and the peak temperatures of the first endothermic valley for aged samples are also smaller than 6# sample; the variety is resulted by the surface and absorption water loss after aging. Similarly, the peak temperatures of the second and third endothermic valley are 690 and 880 °C, which indicate that under high temperature (90 °C) and cumulative dose 0.37 MGy with different dose rate, the influence on the thermal stability and skeleton construction of modified sodium bentonite are almost small. But, the endothermic values of the second endothermic valley for aged samples are also lower (reduced 11–25% compared to 6# sample) than 6# sample.

## 3.3 The X-Ray Diffraction Analyses of Aged Samples

### 3.3.1 The Analyses of Aged Samples

#### 1. The analyses of samples with different accumulative doses

Except the first diffraction peak of low angle, other diffraction peak positions and shapes of the aged samples are basically the same with 6# sample, but the intensities for aged samples are lower than 6# sample, and decrease with the increase of accumulative doses (Figs. 6 and 7). When the accumulative dose is 0.74 MGy, the

**Fig. 6** XRD spectra of Na bentonite with different cumulative dose at 85 Gy/h

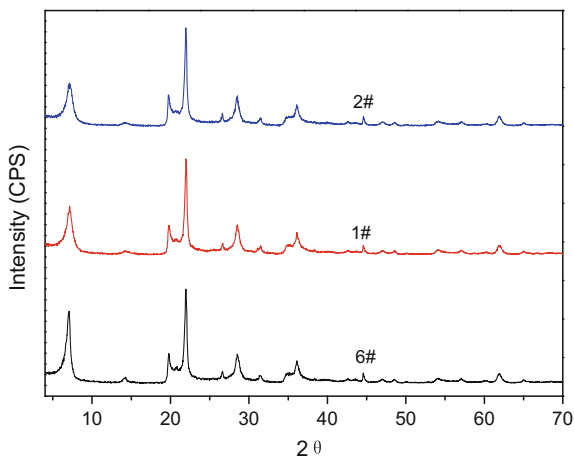
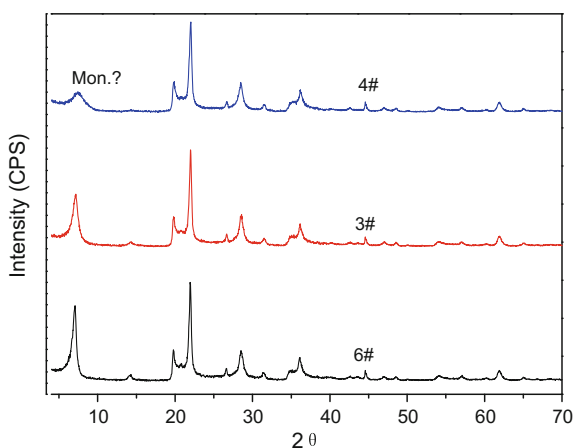


**Fig. 7** XRD spectra of Na bentonite with different cumulative dose at 170 Gy/h



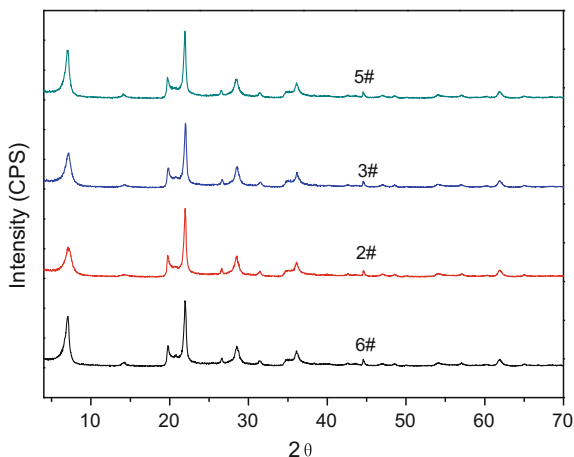
first diffraction peak of low angle is obviously widen, the peak position moves to high angle, and the intensity is lower than 6# sample.

## 2. The analyses of aged samples with the same cumulative dose but different dose rates

It can be seen from Fig. 8, the diffraction peak positions, shapes, and intensities of the aged samples are basically the same with the ones of 6# sample except the (001) diffraction peak of the montmorillonite; after aging, the intensities are lower than that of 6# sample, and decrease with the decrease of the dose rates.

According to the data (Table 3), the first diffraction peak position of 4# sample obviously removes to high angle, the  $d$  space is 11.78 Å, the full width at half maximum (FWHM) is 3.14 times of that for 6# sample, the height reduces 80%,

**Fig. 8** XRD spectra of Na bentonite with different dose rate at 0.37 MGy



and the peak area also reduces 40%; it needs further confirmation whether the peak belongs to new phase caused by the effect of aging. Except that the position and FWHM of (001) diffraction peak of the montmorillonite for 5# sample decrease and d space increase, for other sample, the FWHM increases with increase of cumulative doses under the same dose rate; the d space, peak height and area decrease with increase of cumulative doses under the same dose rate; and the peak height and

**Table 3** Results of quantitative analysis after aging

Samples ID	Phase	(hkl)	2θ (°)	d (Å)	FWHM	Height	Area
6#	Mon.	(001)	7.08	12.47	0.639	1010	31,726
1#	Mon.	(001)	7.17	12.33	0.900	623	25,978
2#	Mon.	(001)	7.19	12.28	0.970	578	25,938
3#	Mon.	(001)	7.10	12.45	0.710	821	28,685
4#	Mon.?	(001)?	7.50	11.78	2.006	226	18,669
5#	Mon.	(001)	7.07	12.49	0.611	975	28,378
6#	Mon.	(060)	61.81	1.50	0.600	148	6178
1#	Mon.	(060)	61.84	1.50	0.597	149	6001
2#	Mon.	(060)	61.84	1.50	0.625	142	5702
3#	Mon.	(060)	61.83	1.50	0.578	152	6002
4#	Mon.?	(060)?	61.82	1.50	0.588	147	5274
5#	Mon.	(060)	61.81	1.50	0.591	147	5875
6#	Cri.	(101)	21.96	4.04	0.308	1386	20,257
1#	Cri.	(101)	21.98	4.04	0.309	1399	21,004
2#	Cri.	(101)	21.96	4.04	0.301	1445	21,828
3#	Cri.	(101)	21.95	4.05	0.303	1415	20,555
4#	Cri.	(101)	21.99	4.04	0.351	1264	20,784
5#	Cri.	(101)	21.93	4.05	0.294	1415	20,530



**Table 4** Water content of Na bentonite after aging

	6#	1#	2#	3#	4#	5#
Water content (%)	8.62	5.37	5.36	5.86	1.64	7.51

area decrease with decrease of dose rate under the same cumulative doses. The  $d_{060}$  space is 1.50 Å for all samples, and there is no formation of trioctahedral minerals [17]. After aging, the position, d space, peak area, and FWHM of the (101) diffraction peak for the cristobalite in all modified sodium bentonite are basically unchanged except 4# sample. For the 4# sample, the FWHM of the (101) diffraction peak becomes widen and peak height decrease.

As previously stated [10], the vary of  $d_{001}$  space for montmorillonite has relation to the water content. One observes in Table 4 that the water content of aged samples is lower than 6# sample especially the 4# sample, and it is in accord with the results of thermal analysis. To validate that the varieties of aged samples under the effect of heating (90 °C) and simultaneously irradiating with different dose rates and cumulative doses are caused by the vary of water content after the affect of aging or transforming new phase, the experiments of the oven-drying (105 °C and 24 h), water uptake in constant temperature and humidity box (25 °C and relative humidity 100%), and natural water absorption were investigated, and then, the samples were studied by XRD.

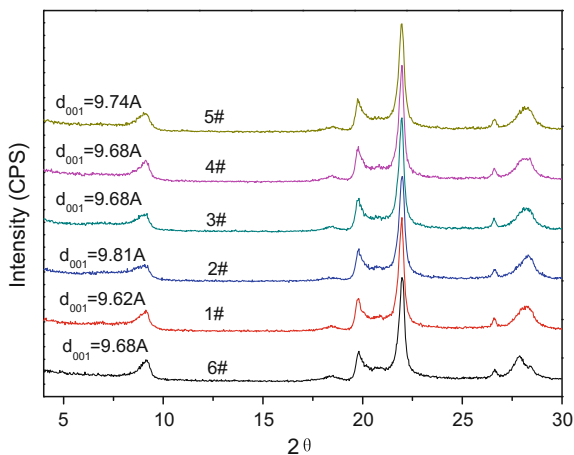
### 3.3.2 The Results of the Samples for Oven-Drying and Water Uptake

For all samples, after oven drying, the shapes positions and intensities of all diffraction peaks are basically the same, the intensities are low and width and the d-spaces are  $(9.72 \pm 0.10)\text{Å}$  (Fig. 9) to the first diffraction peak of low angle. The diffraction spectrum is a basic agreement for all samples after water absorption for 10 min in the constant temperature and humidity box (Fig. 10). As the data (Table 5) shows, the water contents are close and the d-spacings are almost the same ( $12.44 \pm 0.8 \text{ Å}$ ) as that of the first diffraction peak of low angle for all samples. The position and d space of the first diffraction peak of low angle for 4# and 6# sample are close after oven-drying and water uptake in constant temperature and humidity box, but the intensities of 1#, 2#, and 4# sample are lower than that of 6# sample, and the shapes are widen.

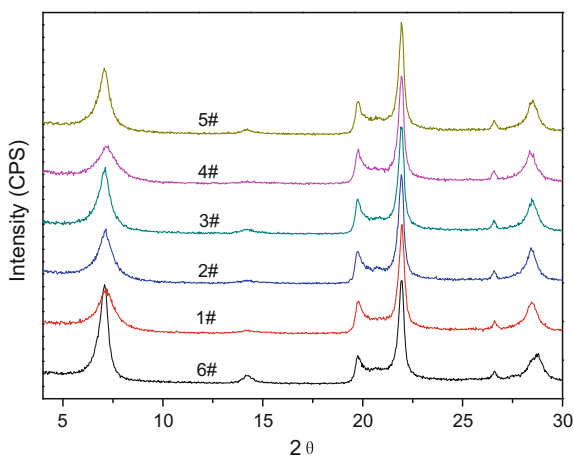
### 3.3.3 The Results of the Samples for Natural Water Uptake

After natural water absorption for 114 days, the intensity for the first diffraction peak of low angle for 4# sample is still lower than that of 6# sample, and the XRD spectrums for other samples are the same with the spectrum of 6# sample (Fig. 11). The data in Table 6 show that the FWHM for the first diffraction peak of low angle is still bigger than that of 6# sample, but smaller than that sample which does not

**Fig. 9** XRD spectra of drying aged Na bentonite



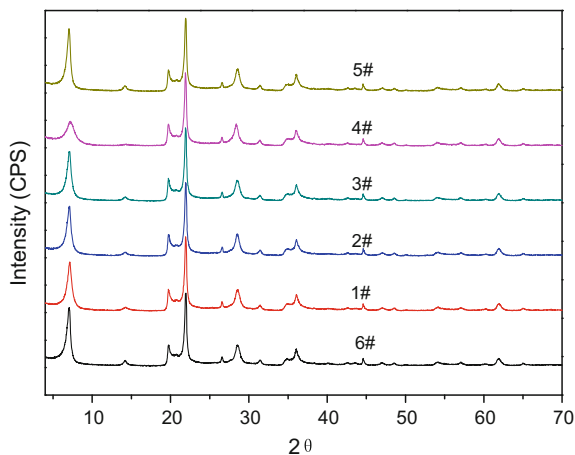
**Fig. 10** XRD spectra of Na bentonite after absorbed water in constant temperature and humidity box



**Table 5** Results of quantitative analysis of aged samples after absorbed water in constant temperature and humidity box

Samples ID	2θ(°)	d <sub>001</sub> (Å)	Water content (%)
6#	7.09	12.46	8.62
1#	7.12	12.40	8.09
2#	7.15	12.36	8.07
3#	7.06	12.51	8.16
4#	7.09	12.46	8.12
5#	7.09	12.46	8.12

absorb water, and the height is up to 36% of 6# sample; it is higher than the sample of nonabsorbent water (22% of 6# sample); the FWHM, heights, and areas of the first diffraction peak of low angle for other aged sample are slightly lower, and this

**Fig. 11** XRD spectra of aged samples after natural absorbed water**Table 6** Results of quantitative analysis of aged samples after natural absorbed water

Samples ID	Phase	(hkl)	2θ (°)	d (Å)	FWHM	Height	Area
6#	Mon.	(001)	7.07	12.49	0.644	3271	13,3947
1#	Mon.	(001)	7.08	12.47	0.644	2723	12,7311
2#	Mon.	(001)	7.14	12.37	0.695	2630	13,0154
3#	Mon.	(001)	7.10	12.44	0.651	2701	123,560
4#	Mon.	(001)	7.21	12.25	1.209	1189	92,648
5#	Mon.	(001)	7.07	12.50	0.632	3363	131,426
6#	Cri.	(101)	21.94	4.05	0.292	4163	90,503
1#	Cri.	(101)	21.94	4.05	0.293	4203	92,648
2#	Cri.	(101)	21.94	4.05	0.297	4160	90,694
3#	Cri.	(101)	21.93	4.05	0.290	4193	90,926
4#	Cri.	(101)	21.91	4.05	0.294	4185	91,489
5#	Cri.	(101)	21.93	4.05	0.289	4233	93,177

**Table 7** Water content of aged samples after natural absorbed water

	6#	1#	2#	3#	4#	5#
Water content (%)	8.62	7.93	7.63	5.78	7.66	8.68

is mostly because that the water content still has some diversity (Table 7). The positions, d-spacing, FWHM, heights, and areas of (101) diffraction peak for cristobalite phase are the same after natural water absorption for 114 days (Table 7).

According to the results of the aged samples, aged samples for oven-drying and water absorption in the constant temperature and humidity box and nature state, the formation of diffraction peak for d space 11.78Å is caused by the decrease in water

content after aging, and it belongs to the (001) diffraction peak of montmorillonite. The varieties of the position, shape and intensity, and FWHM of the first diffraction peak of low angle is caused by the loss of water in the samples under the effect of heating (90 °C) and synchronously irradiating with different dose rates and cumulative doses; the vary is reversible under the aging condition, and there is no visible change of the mineral compositions.

## 4 Conclusions

Thermal analysis, in conjunction with XRD spectrum, was used to study the influence of structure under the effect of heating (90 °C) and synchronously irradiating using different dose rates and cumulative doses in GMZ-modified sodium bentonite. The changes of the first endothermic valley and the first diffraction peak for the low angle were found, but the varieties are reversible after absorbing water again.

In the present study, the influence of heating and irradiating on the thermal properties, phase components, and structures of the GMZ-modified sodium bentonite is no obvious, and the cumulative dose effects and dose rate effects of  $\gamma$  ray are generally weak.

## References

1. Th. Allard and G. Calas. Radiation effects on clay mineral propertise [J]. Applied clay science, 2009, 43:143–149.
2. Th. Allard, E. Balan, G. Calas, et al. Radiation-induced defects in clay minerals: A review [J]. Nuclear instruments and methods in physics research B, 2012, 277:112–120.
3. D. Gournis, A.E. Mantaka-Marketon, M.A. Karakassides, et al. Ionizing radiation-induced defects in smectite clays [J]. Phys Chem Minerals, 2001, 28: 285–290.
4. J. Dies, C. de las Cuevas and F. Tarrasa. The influence of irradiation temperature on the thermoluminescence response of rock salt irradiated in the MGy range [J]. Radiation Protection Dosimetry, 1999, 85:487–492.
5. J. Dies, L. Miralles, F. Tarrasa, J.J. Pueyo, et al. Thermoluminescence response of calcic bentonite subjected to conditions of high nuclear waste underground storage [J]. Radiation Protection Dosimetry, 2002, 100:389–394.
6. R. Pushkareva, E. Kalinichenko, A. Lytovchenko, et al. Irradiation effect on physico-chemical properties of clay minerals [J]. Applied Clay Science, 2002, 21: 117–123.
7. Liang Dong, Liu Wei, Yang Zhontian, et al. A preliminary study on the influences of thermal and  $\gamma$ -rays irradiation aging on modified sodified sodium bentonite [J]. Journal of Radiation Research and Radiation processing. 2012, 30:187–192.
8. R Pusch, O Karnland, A Lajudie et al. MX 80 clay exposed to high temperatures and gamma radiation [R]. SKB Technical Report 93–03, 1992.
9. A.S. Pente, Prema Giresan, R.K. Bajpai, et al. Heat and radiation induced alterations in sorption and swelling characteristics of bentonite clays from north-west India [C]. Nantes, France: 2010. 493–494.

10. Zhao Shuaiwei, Yang Zhontian, Liu Wei, et al. Influences of  $\gamma$ -rays irradiation-thermal sequential aging on the microstructure of modified sodium bentonite [J]. *Journal of Radiation Research and Radiation processing*, 2013, 31: 040403-1-040403-5.
11. M. Plötze and G. Kahr. Alteration of clay minerals—gamma-irradiation effects on physicochemical properties [J]. *Applied Clay Science*, 2003, 23: 195–202.
12. Michael Holmboe, Mats Jonsson. Influence of  $\gamma$ -radiation on there activity of montmorillonite towards  $H_2O_2$  [J]. *Radiation Physics and Chemistry*, 2011.
13. Yang Zhontian, Liang Dong and Liu Wei. Stability of GMZ natural Ca-bentonite and modified Na-bentonite under thermal and electron irradiation aging [J]. *New Chemical Materials*, 2013, 41:112–114.
14. D.T. Reed and D.D. Scott. Gamma and alpha radiation levels in a basalt high-level waste repository: potential impact on container corrosion and packing properties [M]. *Academic Press*, 1987. 325–338.
15. Luo Taian and Liu Xiaodong. Analysis on mineral composition and character of bentonite from the Guangfeng deposit in Jiangxi [J]. *IM & P Industrial Minerals and Processing*. 2004, 10:16–18.
16. D. Gournis, A.E. Mantaka-Marketou, M.A. Karakassides, et al. Effect of  $\gamma$ -irradiation on clays and organoclays: a Mössbauer and XRD study [J]. *Phys Chem Minerals*, 2000, 27:514–521.
17. S. Kaufhold, R. Dohrmann, T. Sanden, et al. Mineralogical investigations of the first package of the alternative buffer material test-I. Alteration of bentonites [J]. *Clay Minerals*, 2013, 8: 199–213.